ACS APPLIED MATERIALS & INTERFACES

Research Article

www.acsami.org

# Highly Active Hydrogen Evolution Electrodes via Co-Deposition of Platinum and Polyoxometalates

Chao Zhang,[†] Yahui Hong,[†] Ruihan Dai,[†] Xinping Lin,[†] La-Sheng Long,[†] Cheng Wang,*[,†] and Wenbin Lin*[,†,‡]

[†]Collaborative Innovation Center of Chemistry for Energy Materials, State Key Laboratory of Physical Chemistry of Solid Surfaces, Department of Chemistry, College of Chemistry and Chemical Engineering, Xiamen University, Xiamen 361005, P. R. China

[‡]Department of Chemistry, University of Chicago, 929 E 57th Street, Chicago, Illinois 60637, United States

Supporting Information

**ABSTRACT:** A highly active hydrogen evolution reaction (HER) electrode with low Pt loading on glassy carbon (GC) has been prepared by anodic platinum dissolution and co-deposition of polyoxometalates. TEM, EDS, XPS, CV, and ICP-MS analyses gave a Pt loading of 50−100 ng/cm$^2$, corresponding to a Pt coverage of only 0.08−0.16 monolayer. With an overpotential of 65 mV at 20 mA/cm$^2$, the modified GC has a HER activity comparable to that of the commercial Pt working electrode.

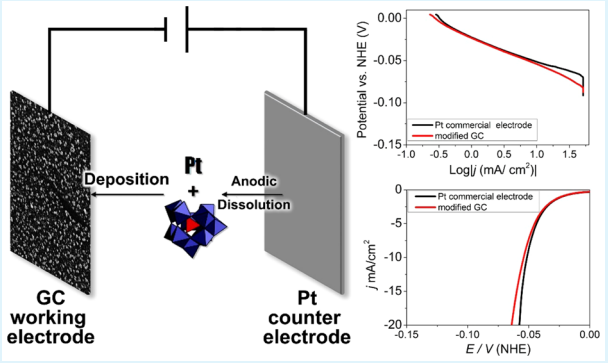


**KEYWORDS:** *hydrogen evolution reaction, anodic platinum dissolution, polyoxometalate*

## 1. INTRODUCTION

Electrochemical production of hydrogen as an energy carrier is an attractive alternative to the current fossil-fuel-centered energy technology.[1−12] Central to the hydrogen cycles are electrocatalysts with high activities and low overpotentials in the hydrogen evolution reaction (HER) and oxygen evolution reaction (OER).[13−15] Platinum, although expensive and with limited global reserves, is still the catalyst of choice for industrial electrolytic cells for HER, due to its superior activity and low overpotential.[16−20] Lowering the amount of Pt needed on the electrodes without sacrificing electrolytic efficiency can thus have immediate and significant implications in the industrial HER processes.[21−28] How to achieve a uniform, stable, and high dispersion of active nanophase catalysts on readily available substrate materials is also key to preparing highly active catalysts for HER and OER processes.[29−32]

Nadjo and Keita published a series of papers on polyoxometalate (POM)-modified electrodes for HER with comparable activity to the Pt electrode.[33,34] The observed activity was later found to come from trace amounts of Pt deposited on the working electrode resulting from anodic dissolution of the Pt counter electrode.[35−39] However, the amount of Pt loading was not accurately determined in the literature, and was roughly estimated to be in the 14−18 μg/cm$^2$ range in one paper.[38] In this work, we performed systematic studies on the preparation of active HER electrodes with extremely low Pt loadings by co-deposition of Pt and POMs via anodic dissolution of the Pt counter electrode. We successfully lowered the Pt loading to the 50−100 ng/cm$^2$ range, 2−3 orders of magnitude lower than the previously reported value, without sacrificing the HER activity. The Pt contents of the electrodes were precisely determined by inductively coupled plasma-mass spectrometry (ICP-MS). Different types of POMs were also investigated in the co-deposition processes. We found that the unsaturated lacunary POM $SiW_{11}O_{39}^{8-}$(denoted as $SiW_{11}$) is superior to the saturated POMs ($SiW_{12}O_{40}^{4-}$ and $P_2W_{18}O_{62}^{6-}$) for HER activities, possibly due to their ability to capture dissolved Pt (presumably Pt(IV)-oxo species)[40] to lead to uniform Pt deposition.

## 2. EXPERIMENTAL SECTION

**2.1. Electrode Preparation.** The electrode was prepared by electrolysis in a typical three-electrode configuration with a CH Instrument-660e electrochemical workstation in a simple single-compartment cell. The reference electrodes were Ag/AgCl (3.5 M KCl) electrodes (+0.2046 V vs NHE). The reference electrode was placed in a position very close to the working electrode. The working electrodes were glassy carbon (GC) discs ($S$ = 0.196 cm$^2$). Before each experiment, the GC electrode was polished to a mirror finish with alumina paste of decreasing grain sizes (0.5 μm to 50 nm). A platinum wire ($d$ = 1 mm, $L$ = 1 cm) was employed as counter electrode. The uncompensated cell resistance was determined from a single-point

Received: April 3, 2015
Accepted: May 12, 2015
Published: May 12, 2015





DOI: 10.1021/acsami.5b02899
ACS Appl. Mater. Interfaces 2015, 7, 11648−11653

high-frequency impedance measurement and was automatically compensated by the built-in positive-feedback software. The 0.5 M $H_2SO_4$ solution was prepared from 18 M $H_2SO_4$ using 18.2 MΩ cm ultrapure water. The electrolyte was degassed with $N_2$ during the electrolysis. $\alpha$-$K_8SiW_{11}O_{39}{\cdot}xH_2O$ ($SiW_{11}$) and $\alpha$-$K_6P_2W_{18}O_{62}{\cdot}xH_2O$ ($P_2W_{18}$) were synthesized according to the literature[41] (see Supporting Information for more details).

**2.2. Determination of the Amount of Pt on the Electrodes.** The Pt loading on the electrode was measured by ICP-MS. Larger GC discs (10 $cm^2$) were used for the electrode preparation in an effort to increase the deposited Pt amounts for the measurements. The surfaces of the prepared electrodes were digested by $HNO_3$:HCl:HF = 1:3:0.05 solution over 12 h. The extraction solution was then diluted to 2% $HNO_3$ and filtered through a 0.22 $\mu$m PTFE filter. The amounts of metals in the solution were determined by ICP-MS, and then used to calculate the amounts of metals on the electrode. ICP-MS was also performed on a smaller GC electrode (0.196 $cm^2$, the same type as in the electrochemical experiments), which gave the density of the deposited Pt at the same order of magnitude as that of the large GC electrode (220 ng/$cm^2$ for the small electrode vs 50−100 ng/$cm^2$ for the large electrode). Although less accurate, the ICP-MS data of the small electrode eliminates the concerns on effects of different deposition area on the deposited Pt density.

## 3. RESULTS AND DISCUSSION

The modified glassy carbon (GC) electrodes were obtained by electrochemical deposition with 1 mM $SiW_{11}O_{39}^{8-}$ and 0.5 M $H_2SO_4$ in the solution and with anodic dissolution of the Pt counter electrode, as shown in Scheme 1. The GC working

**Scheme 1. Electrodeposition of Pt/POM HER Catalysts on GC Surfaces**

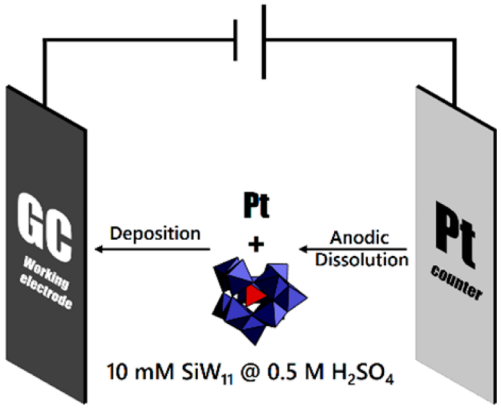


electrode was kept at −0.7 V versus NHE (denoted as **−0.7 V-1 mM-2h-Pt**; see Supporting Information Table S1 for more details) during the deposition. The HER activity of the electrode was examined before and after this co-deposition step by linear sweep voltammetry (LSV) in a fresh 0.5 M $H_2SO_4$ solution without any POM. As shown in Figure 1a, the HER overpotential improved drastically after 2 h of electrolysis (from −844 mV to approximately −340 mV vs NHE @ −20 mA/$cm^2$). The overpotential was further reduced with increasing electrolysis time until it reached −65 mV at −20 mA/$cm^2$ after 12 hours of electrochemical deposition (**−0.7 V-1 mM-12h-Pt**).

The presence of Pt on the working electrode was confirmed by ICP-MS measurements, X-ray photoelectron spectroscopy (XPS), transmission electron microscopy (TEM) imaging and Energy Dispersive X-ray Spectroscopy (EDS) under TEM, which will be discussed in details later. In addition, replacing

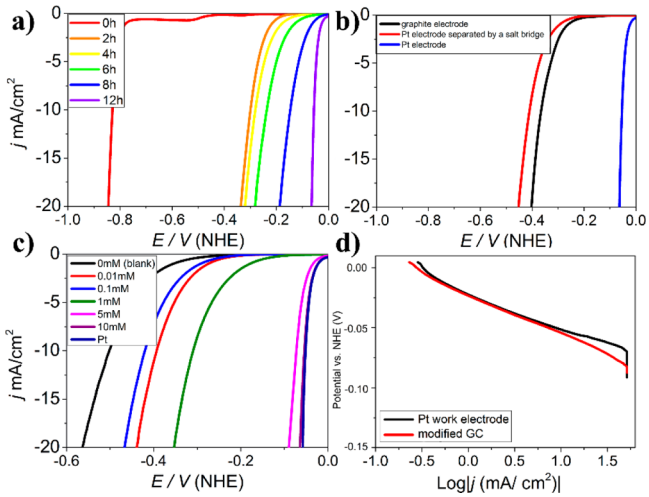


**Figure 1.** (a) LSV curves of modified GCs obtained after different deposition times (**−0.7 V-1 mM-*x*h-Pt, *x*h = 0, 2, 4, 6, 8, 12 h**). (b) LSV curves of modified GCs with different counter electrodes. (c) LSV curves obtained with different concentrations of $SiW_{11}$ in the electrolytic modification step. (d) Tafel plots for Pt electrode and modified GC (**−1.0 V-10 mM-2h-Pt**). Electrolytes: 0.5 M $H_2SO_4$. Scan rate: 5 mV/s.

the Pt counter electrode by a graphite electrode in the electrolysis setup suppressed the HER activity of the modified GC (**-1.0 V-10 mM-2h-G,** Figure 1b), supporting the anodic dissolution as the source of deposited Pt. In line with this observation, separating the working electrode and the Pt counter electrode by a salt bridge in the electrolysis had a similar effect, resulting in suppressed HER activity (Figure 1b). Consistent with the Pt anodic dissolution assumption, a potential difference between the Pt counter electrode and the reference (Ag/AgCl) was measured to be ca. 1.8 V in the experiment (when the potential applied to the working electrode was in the −1.0 V to −0.7 V range vs NHE). The anodic potential of 1.8 V is sufficient to cause some dissolution of Pt to presumably Pt(IV)-oxo species in dilute $H_2SO_4$ solutions.[39,40]

In contrast, the homogeneous $SiW_{11}$ alone does not show significant HER activity above the potential of −800 mV versus NHE on the basis of the LSV, although the reduced POMs were reported to be an HER catalyst with zinc amalgam[42] or a mediator of HER at high concentration.[43] However, the POM co-deposition did play a significant role in the Pt deposition process. The electrode prepared in the absence of POM in solution showed much reduced HER activity (Figure 1c, black curve), although a similar amount of Pt was detected on the GC surface (Table 1). As shown in Figure 1c, the HER activity of the electrode increased with an increasing concentration of POM in the electrolytic deposition solution. When the concentration of $SiW_{11}$ reached 10 mM, the HER activity of the modified GC was comparable to the commercial Pt working electrode (Figure 1 c,d). On the basis of these observations, the co-deposition of POM on the GC electrode either improved the morphology of the deposited Pt for electrocatalysis or enhanced the catalytic activity of Pt.

A sufficiently negative electrolytic potential is necessary in the electrode preparation procedure (Supporting Information Figure S1). When slightly more positive potentials (−0.55 V and −0.2 V vs NHE) were applied to the electrolysis processes, the resultant modified GC electrode was much less active in


DOI: 10.1021/acsami.5b02899
ACS Appl. Mater. Interfaces 2015, 7, 11648−11653

**Table 1. ICP-MS Results of Modified GCs**

| sample | Pt[a,b] (ng/cm$^2$) | W[a,b] (ng/cm$^2$) |
|---|---|---|
| **−1.0 V-0 mM-2h-Pt**[c] | $(6.0 \pm 2.4) \times 10^1$ | – |
| **−1.0 V-10 mM-2h-G** | – | $(6.0 \pm 4.0) \times 10^4$ |
| **−1.0 V-10 mM-2h-Pt** | $(7.6 \pm 2.5) \times 10^1$ | $(1.6 \pm 0.2) \times 10^3$ |
| **−1.0 V-10 mM-2h-G-$K_2PtCl_6$** | $(1.3 \pm 0.6) \times 10^3$ | $(7.2 \pm 3.3) \times 10^2$ |
| **−1.0 V-0 mM-2h-G** | – | – |
| **−1.0 V-0 mM-2h-G-$K_2PtCl_6$** | $(1.0 \pm 0.2) \times 10^3$ | – |

[a]The errors were obtained by parallel preparations of several electrodes and determination of the element contents separately. [b]The entries with dashed lines were measured to be statistically the same as the blank (i.e., within experimental errors). [c]See Supporting Information Table S1 for details of the abbreviations.

HER, even when deposition was carried out for a longer time. For example, with 1 mM $SiW_{11}$ in 0.5 M $H_2SO_4$, 24 h of deposition at −0.2 V (vs NHE) gave an HER overpotential of −740 mV versus NHE @ −20 mA/cm$^2$. By contrast, electrolysis at a more negative potential, e.g., −1.0 V (vs NHE), afforded an electrode with the same activity in a shorter electrolysis time (e.g., the HER activity of **−1.0 V-1 mM-8h-Pt** is equal to **−0.7 V-1 mM-12h-Pt**). Sufficiently negative potential at the working electrode is possibly necessary for the decomposition of POM to achieve beneficial co-deposition. In addition, a sufficiently negative potential also gives relatively large current, which drives up the potential at the counter electrode that is related to anodic dissolution of Pt.

We also tested the feasibility of using $K_2PtCl_6$ (1 $\mu$M) as the Pt source instead of the Pt counter electrode. The Pt wire counter electrode was replaced by graphite electrode in these experiments. In the absence of $SiW_{11}$, after 2 h of electrodeposition (**−1.0 V-0 mM-2h-G-$K_2PtCl_6$**), the HER overpotential was lowered to ca. −200 mV versus NHE @ −20 mA/cm$^2$ (Supporting Information Figure S2), while electrolysis with 10 mM $SiW_{11}$ gives the corresponding HER overpotential of −65 mV (**−1.0 V-10 mM-2h-G-$K_2PtCl_6$**). This result is very similar to that using the Pt counter electrode as the Pt source, but the amount of Pt deposited on the GC electrode to achieve this same HER activity is much more than that of the anodic dissolution method; the amounts of Pt on the modified GCs are $(1.3 \pm 0.6) \times 10^3$ ng/cm$^2$ for $K_2PtCl_6$ deposition and $(6.0 \pm 2.4) \times 10^1$ ng/cm$^2$ for the anodic dissolution method.

In an effort to further investigate the function of POM co-deposition, we tested stepwise deposition of Pt and POM. When Pt was first deposited using $K_2PtCl_6$ (1 $\mu$M) on GC and then followed by POM deposition, we observed decreased HER activity after the POM deposition (Supporting Information Figure S3a). On the other hand, if POM was deposited on GC before the Pt deposition, the HER activity appeared after the Pt deposition step, but no enhancement from POM deposition was observed as compared to the electrode prepared without the first POM deposition step (Supporting Information Figure S3b). These results indicate that the POM must be co-deposited with Pt simultaneously, rather than simply roughing the electrode or forming a base support beforehand, in order to achieve high HER activity with low overpotential. The enhanced HER activity probably results from Pt/POM deposition interfaces that are formed more frequently in the co-deposition process as compared to the stepwise deposition process.

In order to elucidate the form of Pt on the electrode surface, the Tafel plots of $SiW_{11}$/Pt-modified GC (**−1.0 V-10 mM-2h-Pt**) and Pt bulk working electrode were obtained (Figure 1d). These two curves nearly overlapped. The slope for the modified GC was 32 mV/decade, essentially identical to that of the Pt electrode (30 mV/decade), indicating that Pt exists on the electrode surface as metallic nanoparticles or films.[44] The HER exchange current density of the modified GC was ca. $1.9 \times 10^{-4}$ A/cm$^2$. Moreover, the CV of the prepared electrode in 0.5 M $H_2SO_4$ in the potential range between 0.2 and 1.7 V (vs NHE) showed a strong reductive wave at ca. 0.6 V versus NHE, which is identical to the peak associated with formation of a full monolayer of adsorbed oxygen on a typical Pt surface (Supporting Information Figure S4).[45,46] In contrast, the CV of the GC electrode prepared by electrolysis without the Pt source but with POM does not show such features.

The GC electrodes with Pt/POM co-deposition (**−1.0 V-10 mM-2h-Pt**) were examined under scanning electron microscopy (SEM) in order to characterize the morphologies of the deposits. As shown in Figure 2a, nanoparticles with an average

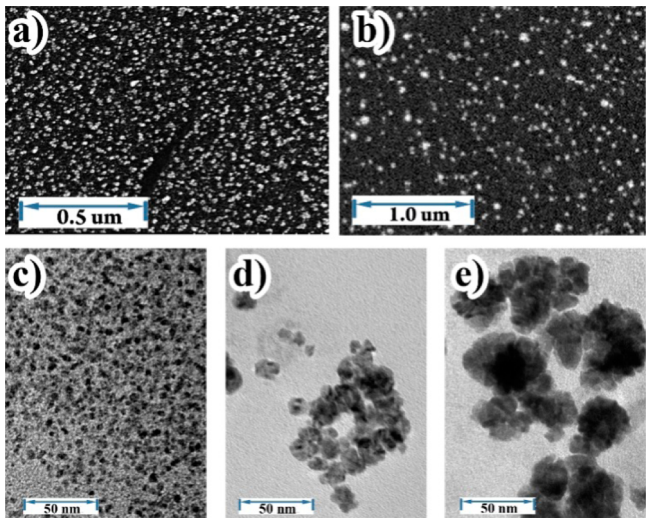


**Figure 2.** SEM images of modified GCs in different methods: (a) (**−1.0 V-10 mM-2h-Pt**) and (b) (**−1.0 V-10 mM-2h-G-$K_2PtCl_6$**). TEM images of the particles separated from the modified GC with different electrolysis durations: (c) 2, (d) 4, and (e) 8 h. Other experimental conditions are the same as those in part a.

diameter of ∼25 nm were observed. EDS analysis revealed that W was the main element of the nanoparticles. No Pt could be detected by EDS, indicating that the Pt loading was below the sensitivity of the EDS technique in the SEM instrument. The electrode prepared with $K_2PtCl_6$ (1 $\mu$M) as the Pt source was also examined (**−1.0 V-10 mM-2h-G-$K_2PtCl_6$**). The diameters of the nanoparticles on the surface of this electrode (∼60 nm) were larger than that of **−1.0 V-10 mM-2h-Pt** (∼25 nm), and Pt was detected on these nanoparticles by EDS (at. 0.13%). We also collected the nanoparticles after sonicating the modified electrode for an extended period and examined them by TEM. As shown in Figure 2c, nanoparticles of 3−5 nm were observed for the sample prepared by 2 h of electrolysis (**−1.0 V-10 mM-2h-Pt**). The smaller particle size under TEM as compared to that in the SEM analysis is possibly due to the sonification step in sample preparation. Longer electrolysis times gave larger nanoparticle sizes (10−20 nm for 4 h, and 35−50 nm for 8 h). Both W and Pt were detected by EDS in these nanoparticles (Supporting Information Table S3). We also observed the lattice fringe image of Pt(111) after 12 h of electrolysis


DOI: 10.1021/acsami.5b02899
ACS Appl. Mater. Interfaces 2015, 7, 11648−11653

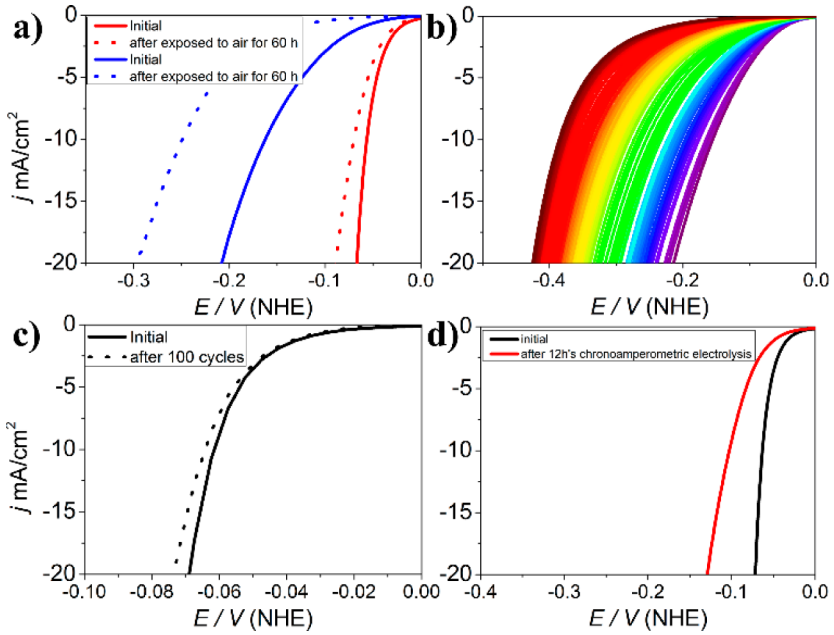


**Figure 3.** (a) LSV curves of modified GCs (**−1.0 V-10 mM-2h-Pt**, red; **−1.0 V-0 mM-2h-Pt**, blue); (b) 100 runs LSV curves of modified GC (**−1.0 V-0 mM-2h-Pt**). (c) LSV curves for a modified GC (**−1.0 V-10 mM-2h-Pt**) initially and after 100 LSV runs; the rest of the curves were omitted for clarity. (d) A comparison of LSV curves for modified GC (**−1.0 V-10 mM-2h-Pt**) before and after 12 h of chronoamperometric electrolysis. Electrolytes: 0.5 M $H_2SO_4$. Scan rate: 5 mV/s.

(Supporting Information Figure S5). Note again that the nanoparticles after 2 h of electrolysis contained insufficient amounts of Pt to be identified by EDS due to the sensitivity issue, but Pt can be clearly identified in larger particles that were obtained after longer electrolysis times.

XPS was also used to characterize the modified GC electrode (**−1.0 V-10 mM-2h-Pt**, Supporting Information Figure S6). We found the binding energies of W $4f_{7/2}$ and W $4f_{5/2}$ to be 36.75 and 38.88 eV, and the binding energy of Si 2p to be 102.87 eV. All of these binding energies are significantly higher than the reported values of silicotungstate.[47] These results indicate that the $SiW_{11}$ may have decomposed during deposition. In addition, we also observed Pt 4f peaks in the XPS, with a measured binding energy of 72.1 eV for Pt $4f_{7/2}$ and 75.4 eV for Pt $4f_{5/2}$. These binding energies are higher than the reported values for metallic Pt and Pt nanoparticles (71.1−71.3 eV for Pt $4f_{7/2}$ and 74.2−74.5 eV for Pt $4f_{5/2}$).[48−51]

The amounts of Pt on the modified GC electrodes were quantified by ICP-MS (Table 1). The Pt loading of the electrode was determined to be 50−100 ng/cm$^2$, 2−3 orders of magnitude smaller than the previously reported values of 14−18 $\mu$g/cm$^2$.[38] This loading is also lower than the values recently reported by Chen and co-workers for Pt monolayers deposited on WC (600 ng/cm$^2$, based on a monolayer of Pt).[21,22] The average Pt thickness was estimated to be only 0.08−0.16 monolayer (based on $\rho_{pt}$ = 21.45 g/cm$^3$, atomic radius: 1.39 Å), but this exhibited comparable HER activity to that of the bulk Pt electrode. The Pt deposition with anodic dissolution of the Pt electrode clearly gave a much lower Pt loading than the use of $K_2PtCl_6$ as the Pt source, but it exhibited comparable HER activity.

The stability of the modified GC electrode was examined in two ways: in air and after repeated HER catalysis. After being electrolyzed with the Pt counter electrode, the modified GC was exposed to air for 60 h. As shown in Figure 3a, the modified GC (**−1.0 V-10 mM-2h-Pt**) exhibited a small decrease in activity (less than 20 mV overpotential increase @ −20 mA/cm$^2$). This result indicates that the Pt/POM-modified GC is stable in air. In comparison, without the co-deposition of $SiW_{11}$, the aerobic stability of the Pt-deposited GC electrode is poor with about 100 mV overpotential increase @ −20 mA/cm$^2$ after 60 h of standing in air (Figure 3a, blue curves). Moreover, we evaluated the stability of the modified GC electrodes by repeating LSV runs in 0.5 M $H_2SO_4$ between 0 V and −0.1 V (vs NHE). After 100 rounds, the GC electrode co-deposited with $SiW_{11}$ and Pt exhibited no measurable loss of HER activity (overpotential @ −20 mA/cm$^2$ increased from −68 to −73 mV, Figure 3c). By contrast, the Pt deposited GC electrode without POM experienced a significant overpotential increase from ca. −210 to ca. −430 mV (Figure 3b). ICP-MS experiments provided an explanation for the drastic difference in stability for the GC electrode co-deposited with $SiW_{11}$ and Pt and the Pt-deposited GC electrode without POM. The amount of Pt on the Pt-deposited GC electrode decreased from 60 ± 24 to 9.7 ± 1.5 ng/cm$^2$ after 100 LSV runs. In contrast, the electrode co-deposited with POM retained the same amount of Pt after 100 LSV runs, showing the stabilization resulted from the POM co-deposition (Supporting Information Table S2). In addition to the degradation studies by repeated LSV scans, we also conducted long-time electrolysis experiments using a Pt/POM-modified GC (modified by **−1.0 V-10 mM-2h-Pt**). The current density decreased with time in blank 0.5 M $H_2SO_4$ at an applied potential of −100 mV versus NHE (Supporting Information Figure S7). The polarization curve after 12 h of electrolysis showed an HER overpotential of ca. −130 mV @ −20 mA/cm$^2$ (Figure 3d), with an increase of 65 mV in overpotential. A similar result was obtained using 1 M $HClO_4$ instead of 0.5 M $H_2SO_4$ as the electrolyte during electrolysis.

To evaluate the Faradaic efficiency for hydrogen evolution, the HER of the Pt/POM-modified GC (**−1.0 V-10 mM-2h-Pt**) was tested in 0.5 M $H_2SO_4$ at −0.7 V versus NHE for 30 s, resulting in the passage of about 1.3 C of charge. The amount


DOI: 10.1021/acsami.5b02899
ACS Appl. Mater. Interfaces 2015, 7, 11648−11653

of $H_2$ was analyzed by gas chromatography and compared with the theoretical volume to give an estimated lower limit Faraday efficiency of 92%. The generated hydrogen is possibly reoxidized on the counter electrode due to the lack of a separator in our electrolysis device, leading to a measured efficiency of less than 100%.

In addition, $H_4SiW_{12}O_{40}{\cdot}xH_2O$ ($SiW_{12}$) and $\alpha$-$K_6P_2W_{18}O_{62}{\cdot}xH_2O$ ($P_2W_{18}$) were also employed as the POMs in the deposition process. As presented in Supporting Information Figure S8, $SiW_{12}$/Pt- and $P_2W_{18}$/Pt-modified GC electrodes gave poorer HER performance than the $SiW_{11}$/Pt-modified one. The questions of how the POM structure may influence the HER activity of modified GC and whether Pt coordination by unsaturated POM is involved in the process are still under investigation.

## 4. CONCLUSIONS

In summary, we have prepared highly active hydrogen evolution electrodes with extremely low Pt coverage of only 0.08−0.16 monolayer by anodic platinum dissolution and co-deposition of polyoxometalates. The co-deposition of POM is found to be crucial for the excellent HER performance of the modified GC, comparable to that of commercial Pt working electrode. Our work establishes an interesting strategy for fabricating highly active HER electrodes using very small amounts of Pt. Such a co-modification strategy presents an opportunity to prepare other hybrid materials with rich interfacial structures to achieve synergistic catalysis with exceptional activities.

## ■ ASSOCIATED CONTENT

### Supporting Information

Summary of electrode modification details; polarization curves; TEM image of observed Pt particles; XPS spectra; EDS results; and electrochemical analyses of $SiW_{11}$, $SiW_{12}$, and $P_2W_{18}$ in 0.5 M $H_2SO_4$. The Supporting Information is available free of charge on the ACS Publications website at DOI: 10.1021/acsami.5b02899.

## ■ AUTHOR INFORMATION

### Corresponding Authors

*E-mail: wangchengxmu@xmu.edu.cn.
*E-mail: wenbinlin@uchicago.edu.

### Author Contributions

The manuscript was written through contributions of all authors. All authors have given approval to the final version of the manuscript.

### Notes

The authors declare no competing financial interest.

## ■ ACKNOWLEDGMENTS

We thank the National Natural Science Foundation of P. R. China (21471126), the National Thousand Talents Program of P. R. China, the 985 Program of Chemistry and Chemical Engineering disciplines of Xiamen University, and the U.S. National Science Foundation (DMR-1308229) for funding. We thank Ms. Ruiyun Huang for administrative help and Prof. Dongping Zhan for insightful discussion.

## ■ REFERENCES

(1) Turner, J. A. Sustainable Hydrogen Production. *Science* **2004**, *305*, 972−974.
(2) Ogden, J. M. Prospects for Building a Hydrogen Energy Infrastructure. *Annu. Rev. Energy* **1999**, *24*, 227−279.
(3) Carmo, M.; Fritz, D. L.; Mergel, J.; Stolten, D. A Comprehensive Review on PEM Water Electrolysis. *Int. J. Hydrogen Energy* **2013**, *38*, 4901−4934.
(4) Nocera, D. G. The Artificial Leaf. *Acc. Chem. Res.* **2012**, *45*, 767−776.
(5) Gray, H. B. Powering the Planet with Solar Fuel. *Nat. Chem.* **2009**, *1*, 112−112.
(6) Walter, M. G.; Warren, E. L.; McKone, J. R.; Boettcher, S. W.; Mi, Q.; Santori, E. A.; Lewis, N. S. Solar Water Splitting Cells. *Chem. Rev.* **2010**, *110*, 6446−6473.
(7) Merki, D.; Hu, X. Recent Developments of Molybdenum and Tungsten Sulfides as Hydrogen Evolution Catalysts. *Energy Environ. Sci.* **2011**, *4*, 3878−3888.
(8) Yuhas, B. D.; Smeigh, A. L.; Douvalis, A. P.; Wasielewski, M. R.; Kanatzidis, M. G. Photocatalytic Hydrogen Evolution from FeMoS-Based Biomimetic Chalcogels. *J. Am. Chem. Soc.* **2012**, *134*, 10353−10356.
(9) Shim, Y.; Young, R. M.; Douvalis, A. P.; Dyar, S. M.; Yuhas, B. D.; Bakas, T.; Wasielewski, M. R.; Kanatzidis, M. G. Enhanced Photochemical Hydrogen Evolution from Fe4S4-Based Biomimetic Chalcogels Containing M2+ (M = Pt, Zn, Co, Ni, Sn) Centers. *J. Am. Chem. Soc.* **2014**, *136*, 13371−13380.
(10) Curtin, P. N.; Tinker, L. L.; Burgess, C. M.; Cline, E. D.; Bernhard, S. Structure−Activity Correlations Among Iridium(III) Photosensitizers in a Robust Water-Reducing System. *Inorg. Chem.* **2009**, *48*, 10498−10506.
(11) Sartorel, A.; Carraro, M.; Scorrano, G.; Zorzi, R. D.; Geremia, S.; McDaniel, N. D.; Bernhard, S.; Bonchio, M. Polyoxometalate Embedding of a Tetraruthenium(IV)-Oxo-Core by Template-Directed Metalation of $[\gamma\text{-}SiW_{10}O_{36}]^{8-}$: A Totally Inorganic Oxygen-Evolving Catalyst. *J. Am. Chem. Soc.* **2008**, *130*, 5006−5007.
(12) Tinker, L. L.; Bernhard, S. Photon-Driven Catalytic Proton Reduction with a Robust Homoleptic Iridium(III) 6-Phenyl-2,2′-Bipyridine Complex ($[Ir(\hat{C}\hat{N}N)_2]^+$). *Inorg. Chem.* **2009**, *48*, 10507−10511.
(13) Garand, E.; Kamrath, M. Z.; Jordan, P. A.; Wolk, A. B.; Leavitt, C. M.; McCoy, A. B.; Miller, S. J.; Johnson, M. A. Determination of Noncovalent Docking by Infrared Spectroscopy of Cold Gas-Phase Complexes. *Science* **2012**, *335*, 694−698.
(14) Sun, Y.; Liu, C.; Grauer, D. C.; Yano, J.; Long, J. R.; Yang, P.; Chang, C. J. Electrodeposited Cobalt-Sulfide Catalyst for Electrochemical and Photoelectrochemical Hydrogen Generation from Water. *J. Am. Chem. Soc.* **2013**, *135*, 17699−17702.
(15) Yang, L.; Zhou, W.; Hou, D.; Zhou, K.; Li, G.; Tang, Z.; Li, L.; Chen, S. Porous Metallic $MoO_2$-Supported $MoS_2$ Nanosheets for Enhanced Electrocatalytic Activity in the Hydrogen Evolution Reaction. *Nanoscale* **2015**, *7*, 5203−5208.
(16) Morales-Guio, C. G.; Stern, L.-A.; Hu, X. Nanostructured Hydrotreating Catalysts for Electrochemical Hydrogen Evolution. *Chem. Soc. Rev.* **2014**, *43*, 6555−6569.
(17) Popczun, E. J.; Read, C. G.; Roske, C. W.; Lewis, N. S.; Schaak, R. E. Highly Active Electrocatalysis of the Hydrogen Evolution Reaction by Cobalt Phosphide Nanoparticles. *Angew. Chem., Int. Ed.* **2014**, *53*, 5427−5430.
(18) Vrubel, H.; Merki, D.; Hu, X. Hydrogen Evolution Catalyzed by $MoS_3$ and $MoS_2$ Particles. *Energy Environ. Sci.* **2012**, *5*, 6136−6144.
(19) Vrubel, H.; Hu, X. Molybdenum Boride and Carbide Catalyze Hydrogen Evolution in Both Acidic and Basic Solutions. *Angew. Chem., Int. Ed.* **2012**, *51*, 12703−12706.
(20) deKrafft, K. E.; Wang, C.; Lin, W. Metal-Organic Framework Templated Synthesis of Fe2O3/TiO2 Nanocomposite for Hydrogen Production. *Adv. Mater.* **2012**, *24*, 2014−2018.
(21) Esposito, D. V.; Chen, J. G. Monolayer Platinum Supported on Tungsten Carbides as Low-Cost Electrocatalysts: Opportunities and Limitations. *Energy Environ. Sci.* **2011**, *4*, 3900−3912.
(22) Esposito, D. V.; Hunt, S. T.; Stottlemyer, A. L.; Dobson, K. D.; McCandless, B. E.; Birkmire, R. W.; Chen, J. G. Low-Cost Hydrogen-


DOI: 10.1021/acsami.5b02899
*ACS Appl. Mater. Interfaces* 2015, 7, 11648−11653

Evolution Catalysts Based on Monolayer Platinum on Tungsten Monocarbide Substrates. *Angew. Chem., Int. Ed.* **2010**, *49*, 9859−9862.
(23) Esposito, D. V.; Hunt, S. T.; Kimmel, Y. C.; Chen, J. G. A New Class of Electrocatalysts for Hydrogen Production from Water Electrolysis: Metal Monolayers Supported on Low-Cost Transition Metal Carbides. *J. Am. Chem. Soc.* **2012**, *134*, 3025−3033.
(24) Gordon, R. B.; Bertram, M.; Graedel, T. E. Metal Stocks and Sustainability. *Proc. Natl. Acad. Sci. U.S.A.* **2006**, *103*, 1209−1214.
(25) Levy, R. B.; Boudart, M. Platinum-Like Behavior of Tungsten Carbide in Surface Catalysis. *Science* **1973**, *181*, 547−549.
(26) Carmo, M.; Fritz, D. L.; Mergel, J.; Stolten, D. A Comprehensive Review on PEM Water Electrolysis. *Int. J. Hydrogen Energy* **2013**, *38*, 4901−4934.
(27) Cook, T. R.; Dogutan, D. K.; Reece, S. Y.; Surendranath, Y.; Teets, T. S.; Nocera, D. G. Solar Energy Supply and Storage for the Legacy and Nonlegacy Worlds. *Chem. Rev.* **2010**, *110*, 6474−6502.
(28) Smith, R. D. L.; Prévot, M. S.; Fagan, R. D.; Zhang, Z.; Sedach, P. A.; Siu, M. K. J.; Trudel, S.; Berlinguette, C. P. Photochemical Route for Accessing Amorphous Metal Oxide Materials for Water Oxidation Catalysis. *Science* **2013**, *340*, 60−63.
(29) Bhowmick, R.; Rajasekaran, S.; Friebel, D.; Beasley, C.; Jiao, L.; Ogasawara, H.; Dai, H.; Clemens, B.; Nilsson, A. Hydrogen Spillover in Pt-Single-Walled Carbon Nanotube Composites: Formation of Stable C−H Bonds. *J. Am. Chem. Soc.* **2011**, *133*, 5580−5586.
(30) Fu, Q.; Li, W.-X.; Yao, Y.; Liu, H.; Su, H.-Y.; Ma, D.; Gu, X.-K.; Chen, L.; Wang, Z.; Zhang, H.; et al. Interface-Confined Ferrous Centers for Catalytic Oxidation. *Science* **2010**, *328*, 1141−1144.
(31) Hu, P.; Duchesne, P. N.; Song, Y.; Zhang, P.; Chen, S. Self-Assembly and Chemical Reactivity of Alkenes on Platinum Nanoparticles. *Langmuir* **2015**, *31*, 522−528.
(32) Lu, X.; Zhao, C. Electrodeposition of Hierarchically Structured Three-Dimensional Nickel−iron Electrodes for Efficient Oxygen Evolution at High Current Densities. *Nat. Commun.***2015**, *6*.
(33) Keïta, B.; Nadjo, L. Activation of Electrode Surfaces: Application to the Lectrocatalysis of the Hydrogen Evolution Reaction. *J. Electroanal. Chem. Interfacial Electrochem.* **1985**, *191*, 441−448.
(34) Keita, B.; Nadjo, L. New Oxometalate-Based Materials for Catalysis and Electrocatalysis. *Mater. Chem. Phys.* **1989**, *22*, 77−103.
(35) Kulesza, P. J.; Faulkner, L. R. Electrocatalysis at a Novel Electrode Coating of Nonstoichiometric tungsten(VI,V) Oxide Aggregates. *J. Am. Chem. Soc.* **1988**, *110*, 4905−4913.
(36) Kulesza, P. J.; Faulkner, L. R. Electrochemical Preparation of Electrodes Modified with Non-Stoichiometric Mixed-Valent tungsten-(VI, V) Oxides. *J. Electroanal. Chem. Interfacial Electrochem.* **1988**, *248*, 305−320.
(37) Kulesza, P. J.; Faulkner, L. R. Electrocatalytic Properties of Bifunctional Pt/W(VI,V) Oxide Microstructures Electrodeposited on Carbon Substrates. *J. Electroanal. Chem. Interfacial Electrochem.* **1989**, *259*, 81−98.
(38) Kulesza, P. J.; Lu, W.; Faulkner, L. R. Cathodic Fabrication of Platinum Microparticles via Anodic Dissolution of a Platinum Counter-Electrode: Electrocatalytic Probing and Surface Analysis of Dispersed Platinum. *J. Electroanal. Chem.* **1992**, *336*, 35−44.
(39) Sadakane, M.; Steckhan, E. Electrochemical Properties of Polyoxometalates as Electrocatalysts. *Chem. Rev.* **1998**, *98*, 219−237.
(40) Rand, D. A. J.; Woods, R. A Study of the Dissolution of Platinum, Palladium, Rhodium and Gold Electrodes in 1 M Sulphuric Acid by Cyclic Voltammetry. *J. Electroanal. Chem. Interfacial Electrochem.* **1972**, *35*, 209−218.
(41) Téazéa, A.; Hervéa, G.; Finke, R. G.; Lyon, D. K. A-, B-, and Γ-Dodecatungstosilicic Acids: Isomers and Related Lacunary Compounds. In *Inorganic Syntheses*; Ginsberg, A. P., Ed.; John Wiley & Sons, Inc.: New York, 1990; pp 85−96.
(42) Savinov, E. N.; Saidkhanov, S. S.; Parmon, V. N.; Zamaraev, K. I. Evolution of Hydrogen from Aqueous Solutions of 12-Silicon-Tungsten Heteropolyacid. *React. Kinet. Catal. Lett.* **1981**, *17*, 407−411.
(43) Rausch, B.; Symes, M. D.; Chisholm, G.; Cronin, L. Decoupled Catalytic Hydrogen Evolution from a Molecular Metal Oxide Redox Mediator in Water Splitting. *Science* **2014**, *345*, 1326−1330.
(44) Bockris, J. O.; Potter, E. C. The Mechanism of the Cathodic Hydrogen Evolution Reaction. *J. Electrochem. Soc.* **1952**, *99*, 169−186.
(45) Climent, V.; Feliu, J. M. Thirty Years of Platinum Single Crystal Electrochemistry. *J. Solid State Electrochem.* **2011**, *15*, 1297−1315.
(46) Angerstein-Kozlowska, H.; Conway, B. E.; Sharp, W. B. A. The Real Condition of Electrochemically Oxidized Platinum Surfaces: Part I. Resolution of Component Processes. *J. Electroanal. Chem. Interfacial Electrochem.* **1973**, *43*, 9−36.
(47) Jun, W.; Zhiyun, W.; Hengbin, Z.; Zhongqing, Z.; Xianren, W.; Quan, W. Synthesis and Properties of Triheteropoly Compounds Containing Mn, Co, Ni. *Chem. J. Chin. Univ.* **1992**, *13*, 1428−1431.
(48) Liu, Z.; Lin, X.; Lee, J. Y.; Zhang, W.; Han, M.; Gan, L. M. Preparation and Characterization of Platinum-Based Electrocatalysts on Multiwalled Carbon Nanotubes for Proton Exchange Membrane Fuel Cells. *Langmuir* **2002**, *18*, 4054−4060.
(49) Moulder, J. F. Stickle, W. F., Sobol, P. E., Bomben, K. D. *Handbook of X Ray Photoelectron Spectroscopy: A Reference Book of Standard Spectra for Identification and Interpretation of Xps Data*; Physical Electronics: Eden Prairie, MN, 1995
(50) Dückers, K.; Bonzel, H. P.; Wesner, D. A. Surface Core Level Shifts of Pt(111) Measured with Y M$\chi$ Radiation (132.3 eV). *Surf. Sci.* **1986**, *166*, 141−158.
(51) Romeo, M.; Majerus, J.; Legare, P.; Castellani, N. J.; Leroy, D. B. Photoemission Study of Pt Adlayers on Ni(111). *Surf. Sci.* **1990**, *238*, 163−168.


DOI: 10.1021/acsami.5b02899
*ACS Appl. Mater. Interfaces* 2015, 7, 11648−11653